The Relative Contributions of Temperature and Moisture to Heat Stress Changes Under Warming

Nicholas J. Lutsko*

Scripps Institution of Oceanography, University of California at San Diego, La Jolla, CA, USA

**Corresponding author address:* Nicholas Lutsko, nlutsko@ucsd.edu

E-mail: nlutsko@ucsd.edu

ABSTRACT

Increases in the severity of heat stress extremes are potentially one of the most impactful consequences of climate change, affecting human comfort, productivity, health and mortality in many places on Earth. Heat stress results from a combination of elevated temperature and humidity, but the relative contributions each of these makes to heat stress changes have yet to be quantified. Here, conditions on the baseline specific humidity are derived for when specific humidity changes will dominate heat stress changes (as measured using the equivalent potential temperature, θ_E), and for when temperature changes will dominate. Separate conditions are derived over ocean and over land, in addition to a condition for when relative humidity changes dominate over the temperature response at fixed relative humidity. These conditions are used to interpret the θ_E responses in transient warming simulations with an ensemble of models participating in the Sixth Climate Model Intercomparison Project. The regional pattern of θ_E changes is shown to be largely determined by the pattern of specific humidity changes, with the pattern of temperature changes playing a secondary role. This holds whether considering changes in mean summertime θ_E or in extreme (98th percentile) θ_E events. Uncertainty in the response of specific humidity to warming is also shown to be the leading source of uncertainty in the θ_E response at most land locations. These results demonstrate that understanding regional changes in specific humidity is largely sufficient for understanding regional changes in heat stress.

1. Introduction

Changes in the severity and duration of extreme heat stress events are potentially one of the most severe impacts of climate change, affecting human health and productivity, and also damaging crops and ecosystems, among many other negative impacts (see Carleton and Hsiang (2016) for discussions of the negative social and economic impacts of extreme heat stress). For large enough global-mean warming, increases in heat stress may even make large parts of the tropics uninhabitable by humans (Sherwood and Huber 2010).

Heat stress is a result of elevated temperature and moisture levels: high temperatures cause more heat to be input into the human body, while high levels of moisture limit the ability of the human body to cool through evaporation, the primary method by which it dissipates excess heat in warm climates. Understanding changes in heat stress in warmer climates thus requires understanding how local temperature and moisture extremes change, and the relative contributions each of these makes to the total change in heat stress.

A warmer climate will have hotter warm-temperature extremes, but it is less clear how changes in moisture will affect heat stress. Simple conceptual models suggest that near-surface relative humidity decreases over land with warming (Byrne and O'Gorman 2016), and this is also robustly seen in observations and in climate model simulations (Simmons et al. (2010); Byrne and O'Gorman (2013); Byrne and O'Gorman (2018)). In terms of specific humidity (q_v), the Clausius-Clapeyron relation implies that q_v will increase by roughly 7%/°C over oceans (where relative humidity changes are small), but the larger relative humidity changes over land mean that q_v will likely increase more slowly than 7%/°C. Instead, changes in q_v over land can be well approximated by assuming the same fractional changes in specific humidity over land as over the ocean source for the land moisture (Chadwick et al. 2016). But these conceptual models of how specific and relative humidity change over land have yet to be connected to changes in heat stress over land, and it is also unclear whether relative or specific humidity is more relevant for quantifying heat stress changes.

Uncertainty in the drivers of heat stress changes is partly a result of the variety of different heat stress metrics, which place differing emphases on the role of moisture (Buzan et al. (2015); Mora et al. (2017); Sherwood (2018)). In the present-day climate, some metrics, such as the wet-bulb temperature (T_w), suggest that low latitude heat stress extremes are dominated by moisture, while other metrics, such as the United States National Weather Service's Heat Index, suggest that tropical and subtropical heat stress extremes are mostly due to temperature extremes (Buzan et al. (2015); Zhao et al. (2015)). Still other metrics, such as the simplified Wet Bulb Globe Temperature show roughly equal contributions from temperature and moisture (Buzan et al. 2015). At a regional scale, Raymond et al. (2017), using T_w as their metric for heat stress, found that moisture extremes tend to dominate heat stress extremes over North America in the present climate, while Wang et al. (2019) showed that the relative contributions of temperature and moisture to T_w extremes over China varies region-by-region.

Changes in temperature and humidity co-vary in climate models, such that intermodel spread in the response of heat stress metrics such as T_w is smaller than if the intermodel spreads in the temperature and (relative or specific) humidity responses were independent (Fischer and Knutti (2012); Buzan and Huber (2020)). The co-variation of changes in temperature and moisture (conditioned on extreme heat stress events) is partly explained by the fact that extreme heat stress generally occurs in the summer, when the atmospheric state is largely determined by convection. Since most atmospheric profiles are close to moist convective neutrality in summer, this places bounds on the possible combinations of temperature, moisture and pressure that can be expected at upper percentile heat stress levels for a given climate state (Buzan and Huber (2020); Zhang and Fueglistaler (2020)). The limited set of possible temperature and moisture values means, for example, that the intensification of extreme warm events is projected to be associated with a reduction in the relative humidity associated with these events, leading to smaller increases in heat stress extremes than in absolute temperature extremes (Coffel et al. 2019). Although the allowable set changes with climate, constituting a "movable limit", convective neutrality provides a useful first-order constraint on the allowable combinations of temperature and moisture for a given climate.

A simple model of the response of heat stress extremes to warming was proposed by Willett and Sherwood (2012), who assumed a uniform shift of summertime Simplified Wet-bulb Globe Temperature (W) and fixed relative humidity to predict changes in regional W extremes. While this model was able to produce a reasonable match to observed W trends over many land regions, the assumption of fixed relative humidity during extreme W events is questionable over land, and the model does not provide an explicit separation of the relative contributions of temperature and moisture. So the relative contributions of temperature and moisture to heat stress changes have still to be separated and quantified.

In this study, conditions are derived on the baseline specific humidity for determining when changes in temperature or in specific humidity can be expected to dominate heat stress changes, with separate conditions over ocean and over land. A further condition is derived for when local relative humidity changes dominate heat stress changes over temperature changes at fixed relative humidity. The arguments focus on equivalent potential temperature (θ_E), because it is conserved under moist pseudoadiabatic ascent and because it is amenable to analysis. Using θ_E also emphasizes specific humidity as the relevant moisture variable. Finally, other metrics of heat stress, such as T_w, scale with θ_E, or at least are strongly influenced by θ_E changes (see Appendix A1). The theory is shown to work well in climate model data, and a key finding is that the pattern of θ_E

changes is well correlated with the pattern of specific humidity changes, whether looking at seasonal changes or at extreme (98th percentile) events. Hence changes in specific humidity explain most of the regional variation in the response of θ_E to warming and, by implication, in the heat stress response.

The theory is presented in the following section. Section 3 then investigates seasonal θ_E changes in 14 models participating in the Sixth Climate Model Intercomparison Project (CMIP6). Included in this section are investigations of the sources of uncertainty in θ_E changes, and of whether the baseline specific humidity can be used to develop emergent constraints on the response of seasonal-mean θ_E. In section 4 changes in extreme (98th percentile) θ_E events are discussed, before the study ends with conclusions in section 5.

2. Theory

a. Over ocean

Equivalent potential temperature can be approximated as (Holton and Hakim 2013):

$$\theta_e \approx \theta \exp\left(\frac{Lq_v}{c_p T_L}\right), \tag{1}$$

where θ is potential temperature, L is the latent heat of warming, q_v is the mixing ratio of water vapor (approximately equal to the specific humidity), c_p is the heat capacity of dry air and T_L is the temperature at the lifting condensation level. Fractional changes in near-surface equivalent potential temperature can be further approximated as

$$\frac{\Delta\theta_e}{\theta_e} \approx \frac{\Delta\theta}{\theta} + \frac{L}{c_p T}\Delta q_v, \tag{2}$$

where the second-order T_L term is ignored, and T_L is approximated by the surface temperature T. (Note that the same final results can be obtained by considering absolute changes in θ_E, rather than fractional changes, but the derivation is slightly clearer when starting with the fractional change.)

If near-surface relative humidity is assumed to stay fixed with warming, then $\frac{\Delta q_v}{q_v} \approx 0.07°\mathrm{C}^{-1}\Delta T$, and substitution into equation 2 gives

$$\frac{\Delta\theta_e}{\theta_e} \approx \frac{\Delta\theta}{\theta} + 0.07°\mathrm{C}^{-1} q_v \frac{L}{c_p}\frac{\Delta T}{T} = \frac{\Delta\theta}{\theta} + 174 q_v \frac{\Delta T}{T}, \tag{3}$$

where q_v denotes the baseline specific humidity. L_v is set to 2.5 $\times 10^6 \mathrm{Jkg}^{-1}$ and c_p to $1005 \mathrm{Jkg}^{-1}°\mathrm{C}^{-1}$, so that $0.07°\mathrm{C}^{-1} \times L_v/c_p \approx 174$. Assuming fractional changes in surface potential temperature are roughly equal to fractional changes in surface temperature (i.e., that surface pressure changes are small, see Appendix A2), the moisture term will dominate the fractional change in θ_e wherever

$$q_v > \frac{1}{174} \approx 5.6 \mathrm{gkg}^{-1} = q_{v,0}.$$

As shown in the following section, this is a low baseline specific humidity threshold, which is met throughout most of the tropics, subtropics and mid-latitudes in summer (see Figure 2d).

For a change in relative humidity of ΔRH, equation 3 is modified to

$$\frac{\Delta\theta_e}{\theta_e} \approx \frac{\Delta\theta}{\theta} + \frac{L}{c_p T}(0.07°\mathrm{C}^{-1} q_v \Delta T + \Delta RH q_v^*) \approx \frac{\Delta\theta}{\theta} + \frac{q_v}{T}\left(174\Delta T + 2490°\mathrm{C}\frac{\Delta RH}{RH}\right). \tag{4}$$

This gives the new approximate condition for moisture to dominate θ_E changes

$$q_v > \left| \frac{1}{174 + \frac{2490°\mathrm{C}}{\Delta\theta}\frac{\Delta RH}{RH}} \right| = q_{v,0}. \tag{5}$$

For an initial relative humidity of 80%, a temperature increase of 2K and an increase in relative humidity of 1%:

$$q_{v,0} = \frac{1}{189} \approx 5.3 \mathrm{gkg}^{-1}.$$

Note that because ΔRH and $\Delta\theta$ can have opposite signs, the two terms in the denominator of equation 5 can cancel, causing $q_{v,0}$ to be undefined. The line of "critical" relative humidity and temperature changes is defined by:

$$\frac{\Delta RH_c}{\Delta\theta_c} = -\frac{174}{2490°\mathrm{C}}RH \approx -0.07°\mathrm{C}^{-1}RH. \qquad (6)$$

Panels a and b of Figure 1 show $q_{v,0}$ for changes in relative humidity of -10% to +10% and temperature changes from -2°C to +10°C, at baseline relative humidities of 60% (panel a) and 80% (panel b). $q_{v,0}$ is very large in a band which stretches from the upper left quadrant of the figure down to the lower right quadrant, for which $\Delta\theta \approx \Delta\theta_c$ and $\Delta RH \approx \Delta RH_c$. $q_{v,0}$ decreases when moving away from this band, with the largest increases when increasing ΔRH at fixed $\Delta\theta$, and $q_{v,0}$ is small for temperature changes close to 0 and lower for a higher baseline relative humidity.

b. Over land

Moisture changes over land can be approximated by assuming fractional changes in specific humidity over land are equal to fractional change in the ocean source from which the land gets its moisture (Chadwick et al. (2016); Byrne and O'Gorman (2016)):

$$\Delta q_{v,L} \approx \gamma \Delta q_{v,O}, \qquad (7)$$

where $\gamma = q_{v,L}/q_{v,O}$. Byrne and O'Gorman (2016) suggest that changes in γ with warming are small, but this result came from an idealized climate model, and changes in vegetation or land-use could lead to large γ responses in the real world. Changes in γ can be incorporated into the theory presented below, but γ will be assumed fixed hereafter to simplify the analysis. Discrepancies between theory and model results in the following sections may be due to γ changes that are not accounted for by the theory.

Repeating the same procedure as before, and assuming fixed relative humidity over the ocean moisture source and fixed γ then gives:

$$\frac{\Delta\theta_{e,L}}{\theta_{e,L}} \approx \frac{\Delta\theta_L}{\theta_L} + 174\gamma q_{v,L}\frac{\Delta T_O}{T_L}, \tag{8}$$

and the moisture term dominates wherever

$$q_{v,L} > \frac{A}{174\gamma}. \tag{9}$$

The amplification factor $A = \Delta T_L/\Delta T_O \approx \Delta\theta_L/\Delta T_O$ and is typically between 1 and 2 (Sutton et al. (2007); Byrne and O'Gorman (2013)), while a typical value of γ in climate model simulations is 0.7 (Byrne and O'Gorman 2016) so that $A/\gamma \approx$ 1.5-3. Hence the baseline specific humidity threshold may be several times higher over land than over ocean.

For a change in relative humidity over the ocean moisture source, equation 9 becomes

$$q_{v,L} > \left| \frac{A}{\gamma\left(174 + \frac{2490^\circ\mathrm{C}}{\Delta\theta_O}\frac{\Delta RH_O}{RH_O}\right)} \right|. \tag{10}$$

The new threshold specific humidity values over land are plotted in panels c and d of Figure 1, again assuming baseline relative humidities of 60% (panel c) and 80% (panel d, note that these represent relative humidities over the oceanic moisture source), and taking γ = 0.7 and A = 1.5. $q_{v,L,0}$ has the same structure as $q_{v,O,0}$, but is larger for a given $\Delta\theta_O$ and ΔRH_O, and also decreases faster with ΔRH_O at a fixed $\Delta\theta_O$.

c. Changes in relative humidity

Equations 5 and 10 provide conditions for when specific humidity changes are the largest contributor to θ_E changes, but relative humidity changes are expected to be small over most ocean locations, so that even if the specific humidity response contributes the most to $\Delta\theta_E$, the response is still driven by the temperature change. To separate the effects of relative humidity changes from the temperature-driven contribution, equations 5 can be re-arranged to give a condition for when relative humidity changes dominate θ_E changes:

$$\left|\frac{\Delta RH}{RH}\right| > \left|\Delta\theta\left(0.07^{\circ}\mathrm{C}^{-1} + \frac{1}{2490^{\circ}\mathrm{C}\times q_v}\right)\right|. \tag{11}$$

For a baseline q_v of 10gkg^{-1} this gives a fractional relative humidity ($\frac{\Delta RH}{RH}$) change of 11%, or 9% for a baseline of 20gkg^{-1}. These are much larger than the relative humidity changes typically seen over oceans, as temperature changes are the main driver of $\Delta\theta_E$ in these regions. The same condition can be used to determine whether local relative humidity changes (ΔRH_L) dominate the θ_E changes over land, rather than warming at fixed relative humidity; however, since non-local processes play an important role in determining land relative humidities, equation 10 may be more useful for understanding the drivers of θ_E changes over land.

3. Seasonal θ_E Changes

To investigate the relative importance of changes in temperature and in specific humidity for θ_E changes, data were taken from simulations with 14 climate models participating in CMIP6 in which CO_2 concentrations were increased at 1%/year (see Table 1 for list of models). For each simulation, $\Delta\theta_E$, $\Delta\theta$ and Δq_v were calculated by taking the difference between averages over years 1-10 and over years 70-80. θ_E was estimated using equation 1, with temperature at the lifting condensation level calculated using equation 21 of Bolton (1980), and multi-model composites were generated by linearly interpolating all of the model responses onto the same 2.5° by 2.5° grid. I focus here on the changes in boreal summer (June-July-August, JJA), because most of the world's population lives in the Northern Hemisphere. Similar results are obtained in other seasons and in the annual-mean, with a notable exception discussed in section 3a. Results are also shown at all latitudes, rather than only in the regions suceptible to extreme heat stress, to more clearly illustrate the different regimes identified by the theory of the previous section.

The JJA multi-model composite clearly shows that changes in moisture dominate the pattern of changes in equivalent potential temperature (compare panels a and c of Figure 2). For example, there are large increases in θ_E over equatorial Africa, particularly along the coastline of the Bay of Guinea, and smaller increases over the Sahara, which match the pattern of specific humidity changes. By contrast, the potential temperature changes over Africa are much more uniform (Figure 2b). Another notable example is in southwest North America, where there is a region of small q_v and θ_E changes stretching southwest-northeast from Baja California into Arizona and New Mexico. This feature is not seen in the potential temperature field. $\Delta\theta_E$ and Δq_v are also strongly correlated throughout the tropical and mid-latitude oceans.

To quantify the correlations, Table 1 gives r^2 values for pattern correlations between $\Delta\theta_E$ and Δq_v, and between $\Delta\theta_E$ and $\Delta\theta$. $\Delta\theta_E$ and Δq_v are very highly correlated in the multi-model composite (r^2 = 0.79), and the average r^2 value across the individual models is 0.76. By contrast, the correlation between $\Delta\theta_E$ and $\Delta\theta$ is weak (r^2 = 0.07) in the multimodel composite, though the correlation with $\Delta\theta$ tends to be higher in individual models (average r^2 = 0.31). Similar results are obtained when the correlations are taken over land areas only (columns 5 and 6 of Table 1), but the correlations with $\Delta q_{v,L}$ are generally higher and the correlations with $\Delta\theta_L$ generally lower. Taking correlations over tropical regiosn only (30°S to 30°N) further increases the correlations with Δq_v and reduces the correlations with $\Delta\theta$ (not shown).

Figure 2d shows the multi-model composite of q_v averaged over years 1-10 of the simulations, which is used as the baseline specific humidity. This is well correlated with $\Delta\theta_E$ in the multi-model composite (r^2 = 0.62), but the correlation is lower in individual models, roughly similar to the correlation with $\Delta\theta$ (average r^2 = 0.33). Considering land areas only improves these correlations (r^2 = 0.73 in the multi-model composite and r^2 averaged over all models = 0.38).

The magenta contours in Figure 2d indicate the 5.6gkg^{-1} isopleth, for which moisture changes will dominate θ_E changes over ocean if relative humidity is fixed. The areas with baseline specific humidities below this threshold include high latitude oceans and desert regions (the Sahara, Arabia, the Kalahari, etc.). For example, the strong warming seen in the Southern Ocean leads to large θ_E changes there, despite small changes in q_v (Figure 2). Over land the temperature-dominated areas will be larger than the area enclosed by the magenta contours because the specific humidity threshold is larger.

To quantify the relative contributions of temperature and moisture, Figure 3a plots the ratio $Q = L_v \Delta q_v / c_p \Delta\theta$ for the multi-model JJA composite. Over oceans there is close agreement with the theory, as the red contours in Figure 3a, which denote where $Q = 1$, closely match the magenta contours in Figure 2d. Over land, Q is less than one over desert regions, with a larger extent than predicted from the magenta contours in Figure 2d, and is also less than one over much of Europe and central Asia, the southern Amazon and central India. Experimenting with other contour levels indicates that over land $q_{v,0}$ varies between 5-10gkg^{-1} (not shown). For example, the North Atlantic experiences the slowest warming of any region, while Europe warms at a similar rate to other land regions at the same latitude (Figure 2b). This suggests that the amplification factor is large over Europe, and temperature dominates the θ_E response even though the baseline specific humidity is relatively high ($\sim$9gkg^{-1}). By contrast, over Australia, southern Africa and the southern part of South America the Q = 1 contours closely follow the $q_{v,0}$ =5.6gkg^{-1} contours.

In summary, although temperature changes dominate the local changes in JJA θ_E over certain land regions, particularly over Eurasia, moisture changes still dominate the pattern of $\Delta\theta_E$. This is because of the much larger regional variation of Δq_v (compare panels b and c of Figure 2), so that changes in θ_E can be approximated as coming from a spatially-homogeneous distribution of potential temperature changes and a spatially-heterogenous pattern of specific humidity changes:

$$\frac{\Delta\theta_E}{\theta_E}(x,y) \approx \frac{\Delta\theta}{\theta} + \frac{L}{c_p T}\Delta q_v(x,y). \tag{12}$$

The greater spatial variation of Δq_v reflects the much larger range of fractional changes in q_v compared to fractional changes in θ: at constant relative humidity a warming of 1°C leads to a 7% increase in specific humidity, but only a ∼0.33%/°C (= 1/300K) increase in temperature. When relative humidity changes are accounted for, fractional changes in specific humidity can vary from ∼0%/°C to more than 7%/°C, whereas the largest fractional changes in temperature will always be less than 1%/°C. Even over the oceans, where relative humidity changes are small and temperature is the main driver of the θ_E response (equation 11), changes in relative humidity are sufficient for the pattern of $\Delta\theta_E$ to be more similar to the pattern of Δq_v than the pattern of $\Delta\theta$.

a. Arctic amplification

The previous section focused on θ_E changes in JJA because most of the land and people on Earth are in the Northern Hemisphere, so this is where the worst impacts of excess heat stress will be experienced. Similar results are found in other seasons – the pattern of $\Delta\theta_E$ primarily determined by the pattern of Δq_v – with the notable exception of boreal winter (December-January-February, DJF; Figure 4). In this season the strong Arctic amplification of warming, combined with the dryness of high latitude winter climates, means that $\Delta\theta_E$ is mostly determined by $\Delta\theta$ at high Northern latitudes and over much of the Northern Hemisphere continents (North America and Eurasia). The pattern correlations between $\Delta\theta_E$ and $\Delta\theta$ are higher in DJF, while the correlation between $\Delta\theta_E$ and Δq_v are lower (not shown). Heat stress extremes are very unlikely to occur in these regions during boreal winter, but this example illustrates that $\Delta\theta$ can play a more important role in determining the pattern of $\Delta\theta_E$ in cold, dry climates, for which the larger absolute changes in θ overcome the larger fractional changes in q_v.

Further south, the θ_E changes in sub-Saharan Africa and South America are primarily dominated by moisture, and in general the 5.6gkg^{-1} threshold accurately separates regions dominated by temperature changes and regions dominated by moisture changes, even over land (compare Figure 3b and Figure 4d).

b. Sources of uncertainty in $\Delta\theta_E$

Uncertainty (intermodel spread) in $\Delta\theta_E$ is due to uncertainties in $\Delta\theta$ and Δq_v. To quantify the contributions of $\Delta\theta$ and Δq_v to uncertainty in $\Delta\theta_E$, Figure 5 shows r^2 values for correlations across models between $\Delta\theta_E$ and $\Delta\theta$ at each grid point (left column) and for correlations between $\Delta\theta_E$ and Δq_v at each grid point (right column). Results are now shown for all seasons, rather than for JJA only, and note that because of correlations between $\Delta\theta$ and Δq_v, the r^2 values at individual grid points can sum to greater than 1. For example, at most ocean locations the r^2 values for both $\Delta\theta$ and Δq_v are close to 1, as relative humidity changes are small and the temperature response is main driver of the q_v and θ_E responses (though $\Delta\theta$ is less well correlated across models with $\Delta\theta_E$ over the equatorial Pacific, implying notable relative humidity changes).

Comparing the left and right columns of Figure 5 shows that at most tropical land locations Δq_v contributes to much more uncertainty in $\Delta\theta_E$ than does uncertainty in $\Delta\theta$. This includes much of South America, sub-Saharan Africa, India, Southeast Asia and Australia. Exceptions include the northern Amazon in DJF (the dry season), the Sahara throughout the year, and southern Australia in SON, where Δq_v and $\Delta\theta$ contribute roughly equal amounts of uncertainty.

At higher latitudes, intermodel variations in $\Delta\theta$ and Δq_v both tend to be well correlated with intermodel variations in $\Delta\theta_E$ over North America and Eurasia, implying that $\Delta\theta$ and Δq_v are also well correlated in these regions. One exception is Europe and Central Asia in JJA, when the r^2 values for $\Delta\theta$ and Δq_v are both near 0.5, suggesting approximately equal contributions to uncertainty in $\Delta\theta_E$ in this season. Δq_v is also poorly correlated with $\Delta\theta_E$ over the Tibetan plateau in boreal winter (Figure 5h).

c. Potential for emergent constraints

The correlations between baseline specific humidity and θ_E changes seen in Figure 2 and quantified in Table 1 hint at the potential for emergent constraints between present-day specific humidity and changes in seasonal-mean θ_E with warming. To investigate this, r^2 values were calculated for correlations across models between the baseline q_v and $\Delta\theta_E$ (Figure 6). Values are only shown over land for ease of presentation and because these regions are of most societal relevance.

In JJA, the baseline specific humidity is poorly correlated with $\Delta\theta_E$ at most locations (Figure 6a), though there are patches of high r^2 values in Equatorial Africa, western South America, parts of the Amazon and over Pakistan. The results of correlations for other seasons are shown in the rest of the Figure, and are similarly patchy, with few large regions of high r^2 values. Sub-Saharan Africa and South America do have patches of high r^2 values in DJF and, interestingly, the warming over much of North America and Eurasia is also well correlated with the baseline q_v in DJF. This suggests that the amplitude of polar amplification could be constrained by the present-day specific humidity, though this has not been investigated further.

Similar results are obtained when $\Delta\theta_E$ is divided by the global-mean surface warming ($\Delta\bar{\theta}$ or $\Delta\bar{T}$) in each model or by local warming ($\Delta\theta(x,y)$). Hence the baseline specific humidity seems to be a poor predictor of future θ_E changes over land. Intermodel variations in the land warming amplification factor (A), in the ratio of land specific humidity to ocean specific humidity (γ), in ΔA and $\Delta\gamma$, and in relative humidity changes could all weaken the connection between baseline specific humidity and $\Delta\theta_E$ in models. At fixed relative humidity, the ratio of the fractional change in θ_E to the fractional change in θ is proportional to q_v:

$$\left(\frac{\Delta\theta_E}{\theta_E}\right) / \left(\frac{\Delta\theta}{\theta}\right) \approx 1 + 174 q_v.$$

This could be used to constrain $\Delta\theta_E$ over ocean regions, given local fractional temperature changes, but will not hold over land regions where relative humidity changes are large.

4. Changes in Extreme Events

Changes in extreme θ_E events are potentially as important as seasonal-mean changes, but the combination of factors driving changes in extreme θ_E events is likely to be more complex. For example, the assumption that fractional changes in moisture over land are equal to the fractional changes in moisture over the relevant oceanic moisture sources may not hold on the synoptic time-scales of extreme heatwaves. Furthermore, soil moisture feedbacks, which are ignored in the theory of section 2, often play a key role in extreme heat stress events (e.g., Diffenbaugh et al. (2007); Donat et al. (2017)). Over oceans, the relative humidities associated with high θ_E events may also have much larger responses to warming than seasonal-mean relative humidities. Nevertheless, the rapid increase of specific humidity with temperature, particularly at warmer temperatures, suggests that specific humidity changes are also likely to be the main driver of extreme θ_E changes.

To investigate the roles of temperature and moisture in changing extreme θ_E events, the analysis of the previous section was repeated for changes in the 98th percentile[1] of the annual distribution of daily θ_E ($\Delta\theta_{E,98}$), with $\Delta\theta$ and Δq_v conditioned on these extreme events ($\Delta\theta_{98}$ and $\Delta q_{v,98}$,

[1]The 98th percentile was chosen as a compromise between capturing "extreme" events and statistical robustness. Similar results are obtained with other percentiles.

respectively) [2]. Comparing Figure 2a and Figure 7a, the magnitudes of $\Delta\theta_{E,98}$ are comparable to the magnitudes of JJA $\Delta\theta_E$, but $\Delta\theta_{E,98}$ is more spatially-uniform, with similar increases over most land locations, whereas JJA $\Delta\theta_E$ is more tropically amplified. There is also less of a land-ocean contrast at high Northern latitudes for $\Delta\theta_{E,98}$.

Just as for the seasonal-mean changes, the pattern of $\Delta\theta_{E,98}$ closely resembles the pattern of moisture changes (Figure 7c). For example, the largest increases in $\Delta\theta_{E,98}$ and in $\Delta q_{v,98}$ over North America are in the Hudson Bay region, with the smallest increases over the southwestern United States and northwestern Mexico. $\Delta\theta_{98}$ is more uniform across North America (Figure 7b), and generally has a smaller magnitude than $\Delta q_{v,98}$. Table 2 confirms this qualitative picture, as $\Delta\theta_{E,98}$ is very highly correlated with $\Delta q_{v,98}$ (r^2 = 0.94 in the multi-model composite, 0.90 in the multi-model mean), and less well correlated with $\Delta\theta_{98}$ (r^2 = 0.30 in the composite, 0.37 in the multi-model mean). Correlations taken over land regions only are similar for $\Delta q_{v,98}$, but lower for $\Delta\theta_{98}$.

$\Delta\theta_{E,98}$ is also well correlated with the baseline $q_{v,98}$ (q_v conditioned on $\theta_{E,98}$ and averaged over years 1-10) in the multi-model composite (Figure 7d), with an r^2 of 0.65. The correlations are generally lower for individual models (multi-model mean r^2 = 0.47), and are similar when taken over land regions only. As with the seasonal-mean θ_E changes, correlations across models between $q_{v,98}$ and $\Delta\theta_{E,98}$ indicate that the conditional baseline specific humidity is a poor constraint on changes in extreme heat stress events at most land locations (not shown).

Even more than the changes in seasonal $\Delta\theta_E$, moisture dominates the response of extreme θ_E events, so that $Q_{98} = L_v \Delta q_{v,98}/c_p \Delta\theta_{98} > 1$ at almost all locations in the tropics, subtropics and mid-latitudes (Figure 8). Exceptions are the Iberian Peninsula, parts of North Africa, Central Asia

[2]Daily surface pressure values were not available for any of the models at the time of the analysis, so the assumption that changes in surface pressure, conditioned on the 98th percentile of daily θ_E, are small has not been verified.

and the southern tip of South America. Extreme θ_E events in these regions are all associated with specific humidities $<10\mathrm{gkg}^{-1}$ in the baseline climate (Figure 7d). Q_{98} is also less than one at high latitudes, where the magenta contour in Figure 7d separates regions of $q_{v,98} > 5.6\mathrm{gkg}^{-1}$ from regions where $q_{v,98} < 5.6\mathrm{gkg}^{-1}$, and closely matches the $Q = 1$ contour in Figure 8.

To demonstrate the importance of specific humidity changes for extreme events in another way, Figure 9 plots the conditional specific humidity and temperature changes for locations over land where the 98th percentile of θ_E in the control climate is above 308K (≈35°C) in the 14 CMIP6 models. The spread in the conditional specific humidity changes is larger than the spread in the conditional temperature changes in almost all of the models, with the exception of some gridpoints in the CanESM5 model. Inspection of the maps of $\Delta\theta_{E,98}$, $\Delta\theta_{98}$ and $\Delta q_{v,98}$ for this model shows that these gridpoints lie over the Tibetan plateau, which experiences large increases in warm, dry events in CanESM5. Otherwise, changes in the very warmest θ_E events are associated in most models with large $q_{v,98}$ responses. For these extreme heat stress events – at or above the limit of what humans can tolerate – the specific humidity response is again the leading factor driving the response to climate change.

Putting this together, the changes in $\theta_{E,98}$ can also be approximated as coming from a spatially-homogeneous distribution of potential temperature changes and a spatially-heterogenous pattern of specific humidity changes:

$$\frac{\Delta\theta_{E,98}}{\theta_{E,98}}(x,y) \approx \frac{\Delta\theta_{98}}{\theta_{98}} + \frac{L}{c_p T_{98}}\Delta q_{v,98}(x,y), \tag{13}$$

so that constraining the regional distribution of extreme θ_E events largely comes down to constraining the changes in the specific humidity associated with these events.

a. Sources of uncertainty in $\Delta\theta_{E,98}$

Specific humidity changes are the primary control on the pattern $\Delta\theta_{E,98}$, suggesting that they also dominate the intermodel spread, or uncertainty, in $\Delta\theta_{E,98}$. Figure 10 repeats the calculations of Figure 5, but now shows correlations across models between $\Delta\theta_{E,98}$ and $\Delta\theta_{98}$ and between $\Delta\theta_{E,98}$ and $\Delta q_{v,98}$. This confirms that $\Delta q_{v,98}$ explains a majority of the intermodel spread in $\Delta\theta_{E,98}$ over most land locations, with high r^2 values for the correlations with $\Delta q_{v,98}$ and low r^2 values for the correlations with $\Delta\theta_{98}$. The most notable exception is parts of the Middle East and Central Asia, where the r^2 values for both $\Delta q_{v,98}$ and $\Delta\theta_{98}$ are between 0.4 and 0.6. This is also where Q_{98} is less than 1 (Figure 8). Other exceptions include northeastern South America, where the r^2 values for both quantities are close to 1, and the Tibetan plateau, where the correlation with $\Delta\theta_{98}$ is high, mostly due to the CanESM5 model.

Over oceans, the potential temperature changes and the specific humidity changes both generally have r^2 values close to 1, implying small relative humidity changes during extreme events, as temperature is the main driver of $\theta_{E,98}$ changes (equation 11). The exception is parts of the tropical and subtropical oceans, where the correlations with $\Delta\theta_{98}$ are lower (r^2 of 0.6-0.8), again implying notable relative humidity changes.

5. Conclusion

There is growing recognition that changes in heat stress could be one of the most devastating consequences of future climate change. Predicting these changes requires climate models that can make accurate prediction of how the many factors involved in extreme heat stress events respond to warming, while also making predictions at the fine scales required to take preventative action. But improved conceptual understanding of the factors governing heat stress changes is also required, to guide the improvement of models and to ensure trust in model results.

In this study, simple conditions on the baseline specific humidity have been derived for when specific humidity can be expected to dominate changes in equivalent potential temperature ($\Delta\theta_E$), with different conditions over ocean and over land. A condition was also derived for when changes in relative humidity dominate the response of θ_E over the response to warming at fixed relative humidity. These conditions have guided an analysis of θ_E changes in transient warming simulations with 14 CMIP6 models. Specific humidity changes are found to be the primary control on the pattern of θ_E changes, whether considering seasonal-mean changes or changes in the 98th percentile of θ_E, so that in both cases the response of $\theta_{E,98}$ can be roughly approximated as coming from a spatially-uniform (i.e., global-mean) potential temperature change and a spatially-varying pattern of specific humidity changes. Specific humidity changes also tend to dominate the intermodel spread, or uncertainty, in $\Delta\theta_E$ over land, particularly for extreme events. Over the oceans, where relative humidity changes are small, the temperature response is the main control on the responses of q_v and θ_E, though relative humidity changes are still large enough for Δq_v to be more highly correlated with $\Delta\theta_E$, particularly in the tropics and subtropics. In summary, improving our understanding of the regional pattern of θ_E changes and reducing the intermodel spread in θ_E, especially over land, can both be largely achieved by understanding and constraining the response of specific humidity to warming.

The key reason for the dominance of specific humidity in θ_E changes is its rapid increase with temperature. Whereas temperature increases by $\sim$0.3%/°C ($\approx 1/300$), specific humidity increases by $\sim$7%/°C at fixed relative humidity. Changes in relative humidity, driven by dynamics, soil moisture feedbacks or land-use changes, can cause the local response of specific humidity to be as low as 0%/°C or to increase faster than the Clausius-Clapeyron scaling. Only in cold, dry climates are the larger fractional increases of specific humidity, and the larger spatial variation in these increases, overwhelmed by temperature increases, so that the pattern of $\Delta\theta$ sets the pattern of $\Delta\theta_E$.

The scalings derived in section 2 imply that $\Delta\theta_E$ is partly determined by the baseline specific humidity, q_v, particularly over oceans. Pattern correlations confirm that q_v and $\Delta\theta_E$ are related, for both seasonal-mean changes and for extreme events, though the correlations tend to be worse in individual models than in the multi-model composite. The relationship between q_v and $\Delta\theta_E$ hints at the potential for emergent constraints, in which present-day specific humidity values are used to constrain future changes in heat stress, but q_v is found to be a poor predictor for changes in $\Delta\theta_E$ over land in the models analyzed here. Intermodel variations in relative humidity, in the land warming amplification factor, in the ratio of specific humidity over ocean to specific humidity over land, and in the responses of these to warming, could obscure the connection between q_v and $\Delta\theta_E$ across models.

More detailed analysis is required to fully understand and constrain the pattern of heat stress changes; to understand local relative humidity changes, how surface processes, such as soil moisture feedbacks, affect local moisture levels, and how the dynamics of synoptic-scale weather events responsible for heat stress extremes change with warming. But the analysis presented above provides a starting point for choosing what to focus on in future investigations. At most locations over land, contraining how the specific humidity during extreme heat stress events respond to global-mean warming is the most important step towards contraining future heat stress changes. Especially for extreme events, the local temperature response plays a secondary role in heat stress changes, and can essentially be set to a single, global-mean value. To put this another way, in most places changes in heat stress will be determined by changes in the body's ability to dissipate excess heat through evaporation, rather than by changes in the amount of heat input into the body.

APPENDIX

A1. Other Heat Stress Metrics

This appendix discusses several other common heat stress metrics whose changes scale similarly to the equivalent potential temperature, θ_E. First, the wet bulb temperature (T_w) is the temperature for a given moist enthalpy at which the relative humidity is 100%:

$$h = c_p T + L q_v = c_P T_w + L q_v^*(T_w), \tag{A1}$$

where q_v^* is the saturation specific humidity. Hence there is a one-to-one correspondance between moist enthalpy and T_w and, assuming surface pressure changes are small, between ΔT_w and $\Delta\theta_E$.

Next, the Wet Bulb Globe Temperature ($WBGT$) is given by (Willett and Sherwood 2012):

$$WBGT = 0.7T_w + 0.2T_g + 0.1T \tag{A2}$$

where T_g is the black globe temperature: the temperature of a sensor placed in the center of a black globe, so that the temperature of the sensor is only determined by the radiation absorbed by the black globe. Thus, $\Delta WBGT$ is mostly set by ΔT_w, though changes in the black globe temperature and in air temperature also contribute, so that specific humidity is relatively less important than for ΔT_w.

Finally, the Simplified Wet Bulb Globe Temperature (W) is defined as (Willett and Sherwood 2012):

$$W = 0.567T + 0.393e + 3.94, \tag{A3}$$

where e is the vapor pressure in hPa. Substituting $q_v \approx 0.622\frac{e}{P_s}$, where P_s is surface pressure in hPa, and assuming a fixed surface pressure of 1000hPa, the change in W is:

$$\Delta W \approx 0.567\Delta T + 622\Delta q_v. \tag{A4}$$

At fixed relative humidity $\Delta q_v \approx 0.07 q_v \Delta T$, and

$$\Delta W \approx 0.567 \Delta T + 43.54 q_v \Delta T. \tag{A5}$$

Hence at fixed relative humidity moisture changes dominate changes in W wherever the baseline specific humidity

$$q_v > \frac{1}{77} \approx 13 \mathrm{gkg}^{-1}. \tag{A6}$$

This condition can be adjusted for relative humidity changes and for land conditions following the same procedure as sections 2b and 2c. Higher baseline specific humidity values are thus required for moisture to dominate changes in W.

A2. Surface Pressure Changes

The multi-model composite changes in JJA surface pressure are shown in Figure 11. The largest changes in surface pressure are located off the coast of Antarctica, with values of up to ~0.7hPa. Given typical surface pressures of O(1000hPa), these represent fractional changes of less than 0.1%. Similar orders of magnitude are obtained for individual models, in other seasons and in the annual-mean.

Acknowledgment. I thank Daniel Koll, Max Popp, Michael Byrne, Yi Zhang, Stephan Fueglistaler and Karen McKinnon for helpful conversations and comments over the course of this project.

References

Bolton, D., 1980: The computation of equivalent potential temperature. *Monthly Weather Review*, **108**, 1046–1053.

Buzan, J. R., and M. Huber, 2020: Moist Heat Stress on a Hotter Earth. *Annual Review of Earth and Planetary Sciences*, **48 (1)**, null.

Buzan, J. R., K. Oleson, and M. Huber, 2015: Implementation and comparison of a suite of heat stress metrics within the Community Land Model version 4.5. *Geoscientific Model Development*, **8 (2)**, 151–170.

Byrne, M. P., and P. A. O'Gorman, 2013: Link between landocean warming contrast and surface relative humidities in simulations with coupled climate models. *Geophysical Research Letters*, **40 (19)**, 5223–5227.

Byrne, M. P., and P. A. O'Gorman, 2016: Understanding Decreases in Land Relative Humidity with Global Warming: Conceptual Model and GCM Simulations. *Journal of Climate*, **29 (24)**, 9045–9061.

Byrne, M. P., and P. A. O'Gorman, 2018: Trends in continental temperature and humidity directly linked to ocean warming. *Proceedings of the National Academy of Sciences*, **115 (19)**, 4863–4868.

Carleton, T. A., and S. M. Hsiang, 2016: Social and economic impacts of climate. *Science*, **353 (6304)**, aad9837–aad9837.

Chadwick, R., P. Good, and K. Willett, 2016: A Simple Moisture Advection Model of Specific Humidity Change over Land in Response to SST Warming. *Journal of Climate*, **29 (21)**, 7613–7632.

Coffel, E. D., R. M. Horton, J. M. Winter, and J. S. Mankin, 2019: Nonlinear increases in extreme temperatures paradoxically dampen increases in extreme humid-heat. *Environmental Research Letters*, **14**, 084 003.

Diffenbaugh, N. S., J. S. Pal, F. Giorgi, and X. Gao, 2007: Heat stress intensification in the Mediterranean climate change hotspot. *Geophysical Research Letters*, **34 (11)**, L11 706.

Donat, M. G., A. J. Pitman, and S. I. Seneviratne, 2017: Regional warming of hot extremes accelerated by surface energy fluxes. *Geophysical Research Letters*, **44 (13)**.

Fischer, E. M., and R. Knutti, 2012: Robust projections of combined humidity and temperature extremes. *Nature Climate Change*, **3**, 126–130.

Holton, J. R., and G. J. Hakim, 2013: *An Introduction to Dynamic Meteorology*. 5th ed., Academic Press.

Mora, C., and Coauthors, 2017: Global risk of deadly heat. *Nature Climate Change*, **7 (7)**, 501–506.

Raymond, C., D. Singh, and R. M. Horton, 2017: Spatiotemporal Patterns and Synoptics of Extreme Wet-Bulb Temperature in the Contiguous United States. *Journal of Geophysical Research: Atmospheres*, **122 (24)**, 13,108–13,124.

Sherwood, S. C., 2018: How Important Is Humidity in Heat Stress? *Journal of Geophysical Research: Atmospheres*, **123 (21)**, 11,808–11,810.

Sherwood, S. C., and M. Huber, 2010: An adaptability limit to climate change due to heat stress. *Proceedings of the National Academy of Sciences*, **107 (21)**, 9552–9555.

Simmons, A. J., K. M. Willett, P. D. Jones, P. W. Thorne, and D. P. Dee, 2010: Low-frequency variations in surface atmospheric humidity, temperature, and precipitation: Inferences from reanalyses and monthly gridded observational data sets. *Journal of Geophysical Research: Atmospheres*, **115 (D1)**.

Sutton, R. T., B. Dong, and J. M. Gregory, 2007: Land/sea warming ratio in response to climate change: IPCC AR4 model results and comparison with observations. *Geophysical Research Letters*, **34 (2)**.

Wang, P., L. R. Leung, J. Lu, F. Song, and J. Tang, 2019: Extreme Wet-Bulb Temperatures in China: The Significant Role of Moisture. *Journal of Geophysical Research: Atmospheres*, **124 (22)**, 11 944–11 960.

Willett, K. M., and S. Sherwood, 2012: Exceedance of heat index thresholds for 15 regions under a warming climate using the wet-bulb globe temperature. *International Journal of Climatology*, **32 (2)**, 161–177.

Zhang, Y., and S. Fueglistaler, 2020: How Tropical Convection Couples High Moist Static Energy Over Land and Ocean. *Geophysical Research Letters*, **47 (2)**, e2019GL086 387.

Zhao, Y., A. Ducharne, B. Sultan, P. Braconnot, and R. Vautard, 2015: Estimating heat stress from climate-based indicators: present-day biases and future spreads in the CMIP5 global climate model ensemble. *Environmental Research Letters*, **10 (8)**, 084 013.

LIST OF TABLES

TABLE 1. r^2 values for correlations between JJA $\Delta\theta_E$ and JJA $\Delta\theta$, JJA $\Delta\theta_E$ and JJA Δq_v and JJA $\Delta\theta_E$ and JJA q_v, as well as r^2 values for the same correlations taken over land regions only. Bold values have a p-value less than 0.025, which gives an estimate of the statistical significance of the correlations.

Model	r^2 ($\Delta\theta_E$, $\Delta\theta$)	r^2 ($\Delta\theta_E$, Δq_v)	r^2 ($\Delta\theta_E$, q_v)	r^2 ($\Delta\theta_{E,L}$, $\Delta\theta_L$)	r^2 ($\Delta\theta_{E,L}$, $\Delta q_{v,L}$)	r^2 ($\Delta\theta_{E,L}$, $q_{v,L}$)
CanESM5	**0.22**	**0.88**	**0.49**	0.19	**0.86**	**0.51**
CESM2	**0.28**	**0.77**	**0.45**	0.17	**0.86**	**0.59**
CESM2-WACCM	**0.22**	**0.70**	**0.35**	0.02	**0.79**	**0.40**
CNRM-CM6-1	**0.43**	**0.63**	0.13	0.24	**0.59**	0.15
CNRM-ESM1	**0.52**	**0.69**	0.11	**0.39**	**0.56**	0.06
EC-Earth3-Veg	**0.23**	**0.77**	**0.33**	0.18	**0.83**	**0.41**
GFDL-CM4	**0.40**	**0.78**	**0.32**	**0.37**	**0.82**	**0.38**
GFDL-ESM4	**0.32**	**0.80**	**0.46**	0.19	**0.84**	**0.53**
HadGEM3-GC31-LL	**0.29**	**0.73**	**0.26**	**0.42**	**0.87**	**0.35**
IPSL-CM6A-LR	**0.20**	**0.79**	**0.39**	0.08	**0.72**	0.33
MIROC-ES2L	**0.29**	**0.87**	**0.50**	0.11	**0.82**	**0.55**
MRI-ESM2-0	**0.43**	**0.67**	0.11	0.22	**0.54**	0.11
SAM0-UNICON	**0.19**	**0.81**	**0.46**	0.11	**0.86**	**0.59**
UKESM1-0-LL	**0.33**	**0.72**	**0.24**	**0.40**	**0.82**	0.31
Multi-model mean	0.31	0.76	0.33	0.22	0.77	0.38
Multi-model composite	0.07	**0.79**	**0.57**	0.00	**0.91**	**0.73**

TABLE 2. r^2 values for correlations between $\Delta\theta_{E,98}$ and $\Delta\theta_{98}$, $\Delta\theta_{E,98}$ and $\Delta q_{v,98}$ and $\Delta\theta_{E,98}$ and $q_{v,98}$, as well as r^2 values for the same correlations taken over land regions only. Bold values have a p-value less than 0.025, which gives an estimate of the statistical significance of the correlations.

Model	r^2 ($\Delta\theta_{E,98}$, $\Delta\theta_{98}$)	r^2 ($\Delta\theta_{E,98}$, $\Delta q_{v,98}$)	r^2 ($\Delta\theta_{E,98}$, $q_{v,98}$)	r^2 ($\Delta\theta_{E,98,L}$, $\Delta\theta_{98,L}$)	r^2 ($\Delta\theta_{E,98,L}$, $\Delta q_{v,98,L}$)	r^2 ($\Delta\theta_{E,98,L}$, $q_{v,98,L}$)
CanESM5	**0.31**	**0.93**	**0.54**	0.11	**0.90**	**0.56**
CESM2	**0.33**	**0.92**	**0.56**	0.12	**0.88**	**0.49**
CESM2-WACCM	**0.27**	**0.85**	**0.40**	0.11	**0.75**	0.20
CNRM-CM6-1	**0.23**	**0.89**	**0.64**	0.04	**0.86**	**0.64**
CNRM-ESM1	**0.31**	**0.91**	**0.68**	0.17	**0.85**	**0.68**
EC-Earth3-Veg	**0.45**	**0.88**	**0.20**	**0.38**	**0.87**	0.21
GFDL-CM4	**0.57**	**0.92**	**0.45**	**0.51**	**0.89**	**0.47**
GFDL-ESM4	**0.38**	**0.88**	**0.50**	0.23	**0.80**	0.48
HadGEM3-GC31-LL	**0.40**	**0.92**	**0.48**	**0.43**	**0.92**	0.55
IPSL-CM6A-LR	**0.45**	**0.91**	**0.45**	**0.44**	**0.90**	**0.47**
MIROC-ES2L	**0.59**	**0.94**	**0.39**	**0.45**	**0.93**	**0.50**
MRI-ESM2-0	**0.25**	**0.79**	**0.32**	0.06	**0.60**	0.26
SAM0-UNICON	**0.37**	**0.92**	**0.55**	0.21	**0.88**	**0.53**
UKESM1-0-LL	**0.39**	**0.90**	**0.42**	**0.38**	**0.90**	**0.49**
Multi-model mean	0.37	0.90	0.47	0.26	0.85	0.47
Multi-model composite	**0.30**	**0.94**	**0.65**	0.15	**0.95**	**0.69**

LIST OF FIGURES

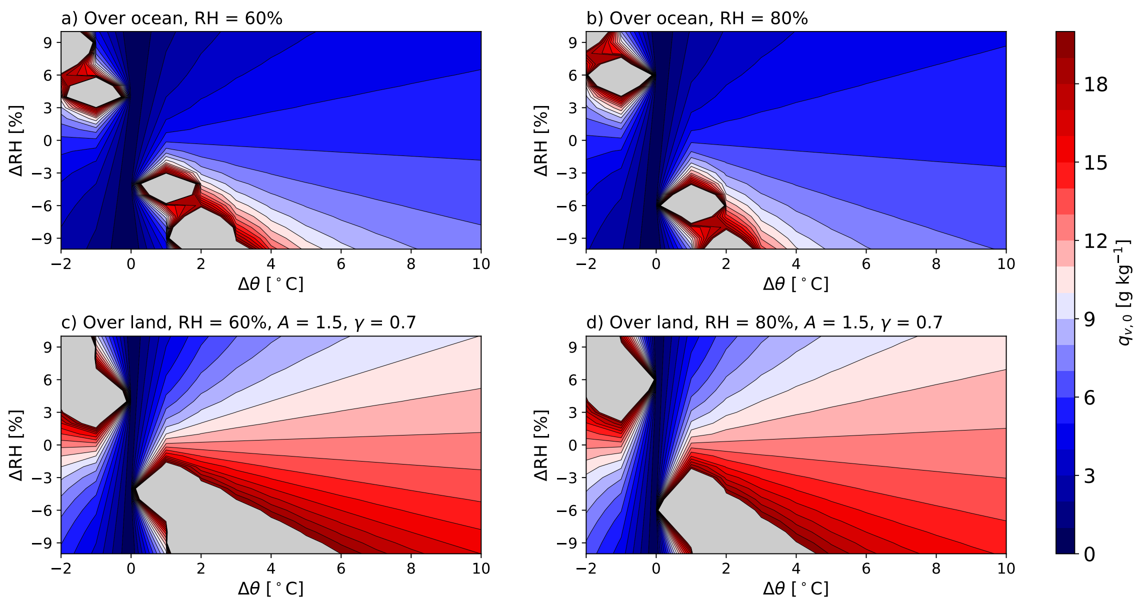

FIG. 1. a) The baseline specific humidity $q_{v,0}$ above which moisture changes dominate changes in θ_E over ocean as a function of $\Delta\theta$ and ΔRH, for a baseline relative humidity of 60%. The values of $q_{v,0}$ are calculated using equation 5. b) Same as a), but assuming a baseline relative humidity of 80%. c) Same as panel a), but showing the baseline specific humidity $q_{v,0}$ over land (i.e., equation 10), assuming a land warming amplification factor A of 1.5. d) Same as panel c), but assuming a baseline relative humidity of 80%. In all panels, the gray shading denotes values of $q_{v,0}$ outside the colorbar scale.

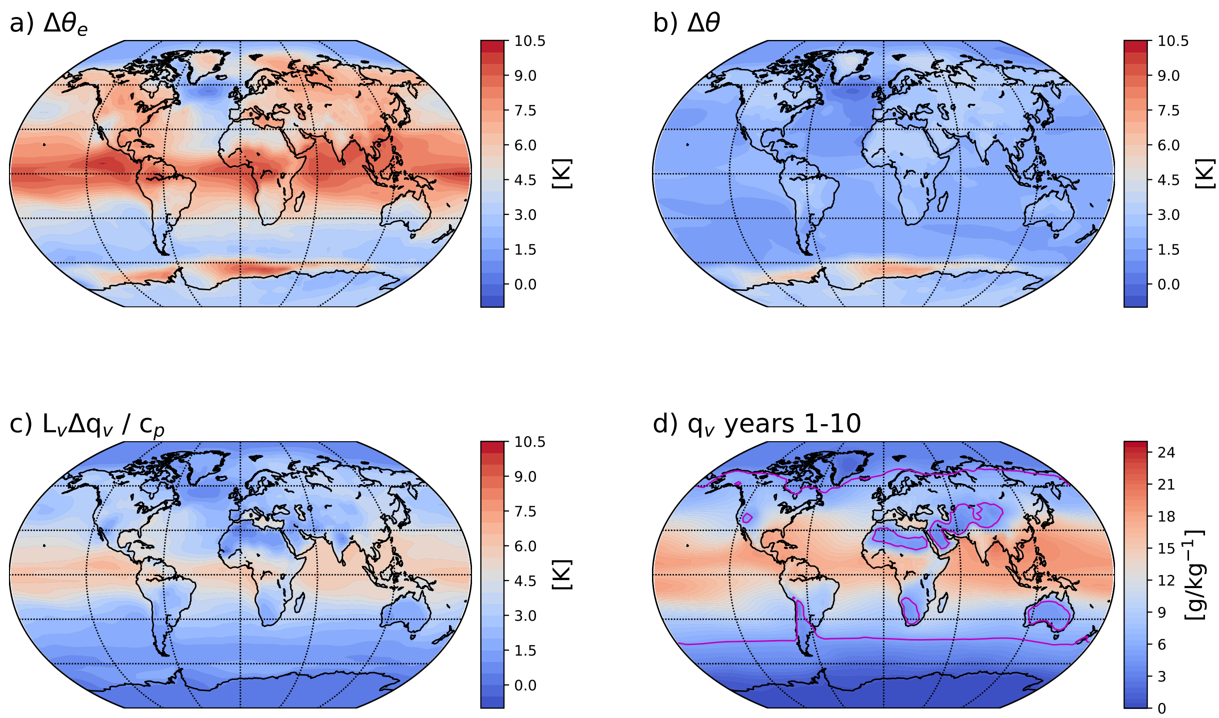

FIG. 2. a) Composite changes in JJA θ_E between years 71-80 and years 1-10 in transient warming simulations with 14 CMIP6 models. b) Composite changes in JJA θ. c) Composite changes in JJA q_v, mulitplied by $\frac{L_v}{c_p}$. d) Composite of JJA q_v, averaged over years 1 - 10 of the simulations. The magenta contours show the 5.6gkg^{-1} isopleth.

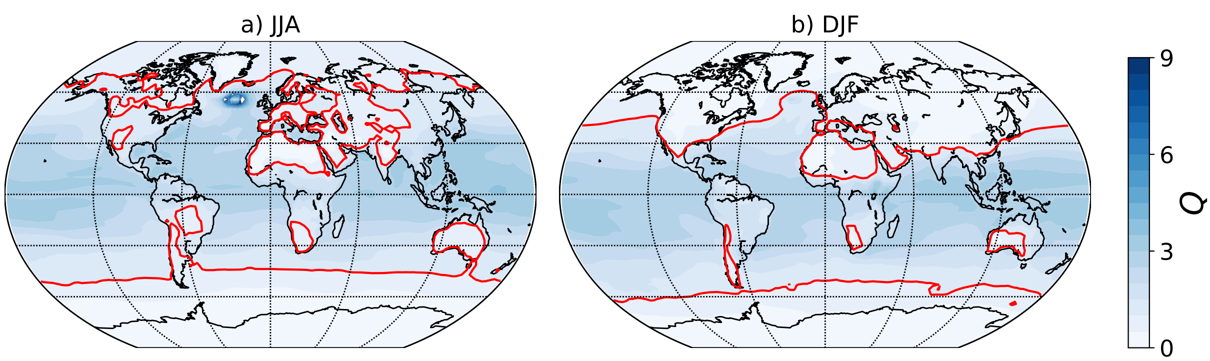

FIG. 3. a) The ratio $Q = L_v \Delta q_v / c_p \Delta\theta$ for the multi-model composite response of the 14 CMIP6 models. b) Same as panel a) but for DJF.

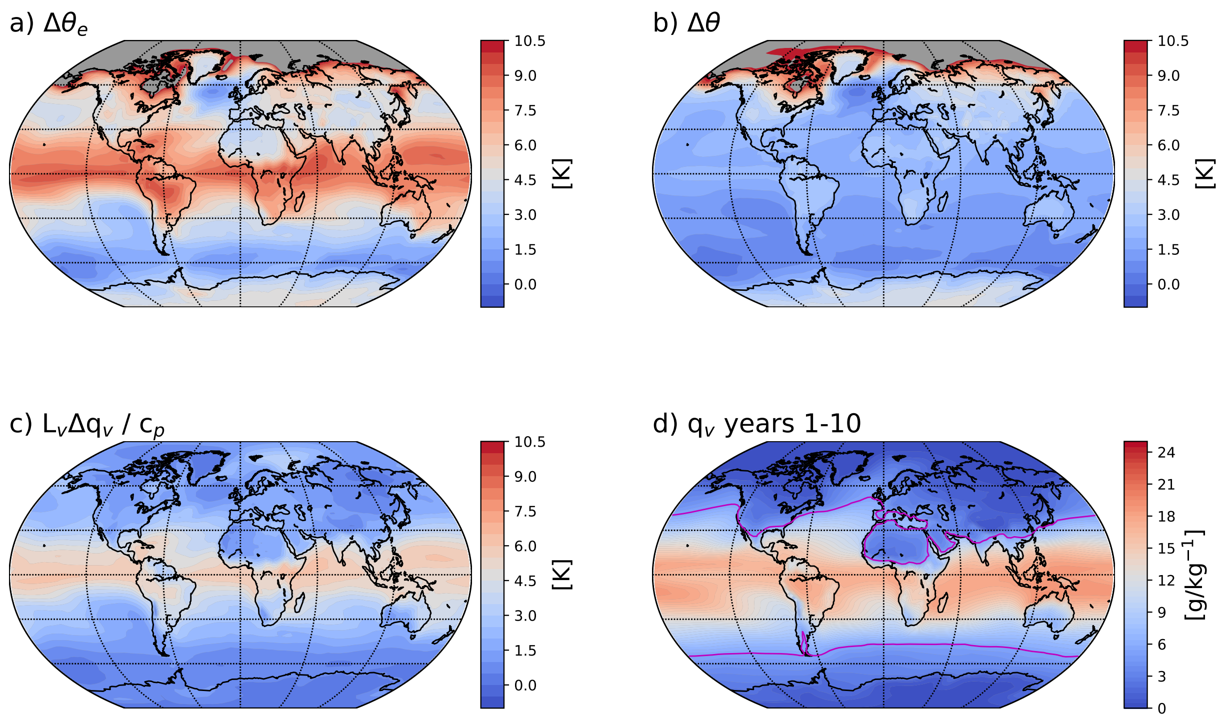

FIG. 4. a) Composite changes in DJF θ_E between years 71-80 and years 1-10 in transient warming simulations with 14 CMIP6 models. b) Composite changes in DJF θ. c) Composite changes in DJF q_v, mulitplied by $\frac{L_v}{c_p}$. d) Composite of DJF q_v, averaged over years 1 - 10 of the simulations. The magenta contours show the 5.6gkg^{-1} isopleth. In all panels, the gray shading denotes values outside the colorbar scales.

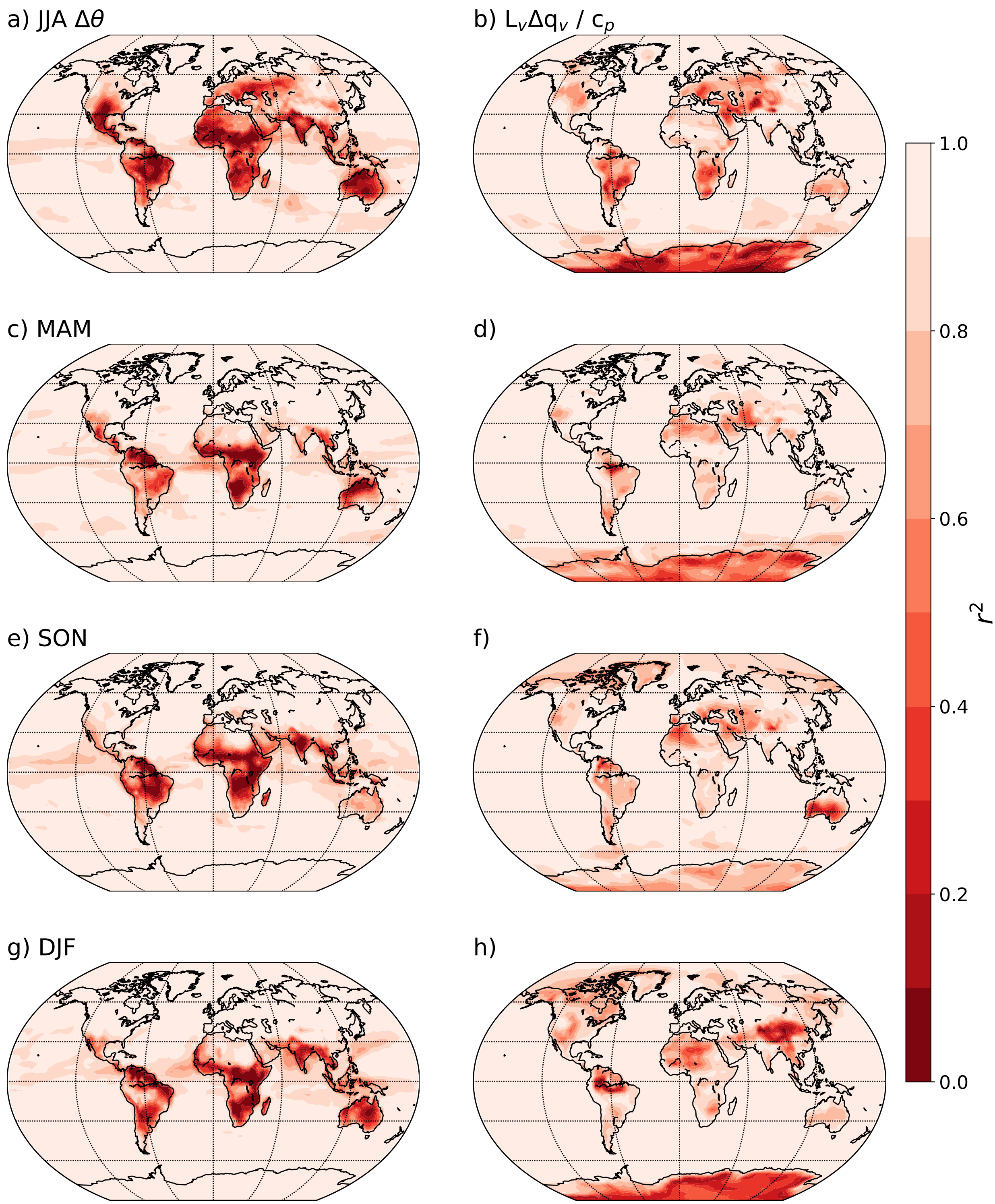

FIG. 5. a) r^2 values for correlations across the CMIP6 models between JJA $\Delta\theta_E$ and JJA $\Delta\theta$. b) r^2 values for correlations across the CMIP6 models between JJA $\Delta\theta_E$ and JJA Δq_v. c) Same as panel a) but for MAM. d) Same as panel b) but for MAM. e) Same as panel a) but for SON. f) Same as panel b) but for SON. g) Same as panel a) but for DJF. h) Same as panel b) but for DJF.

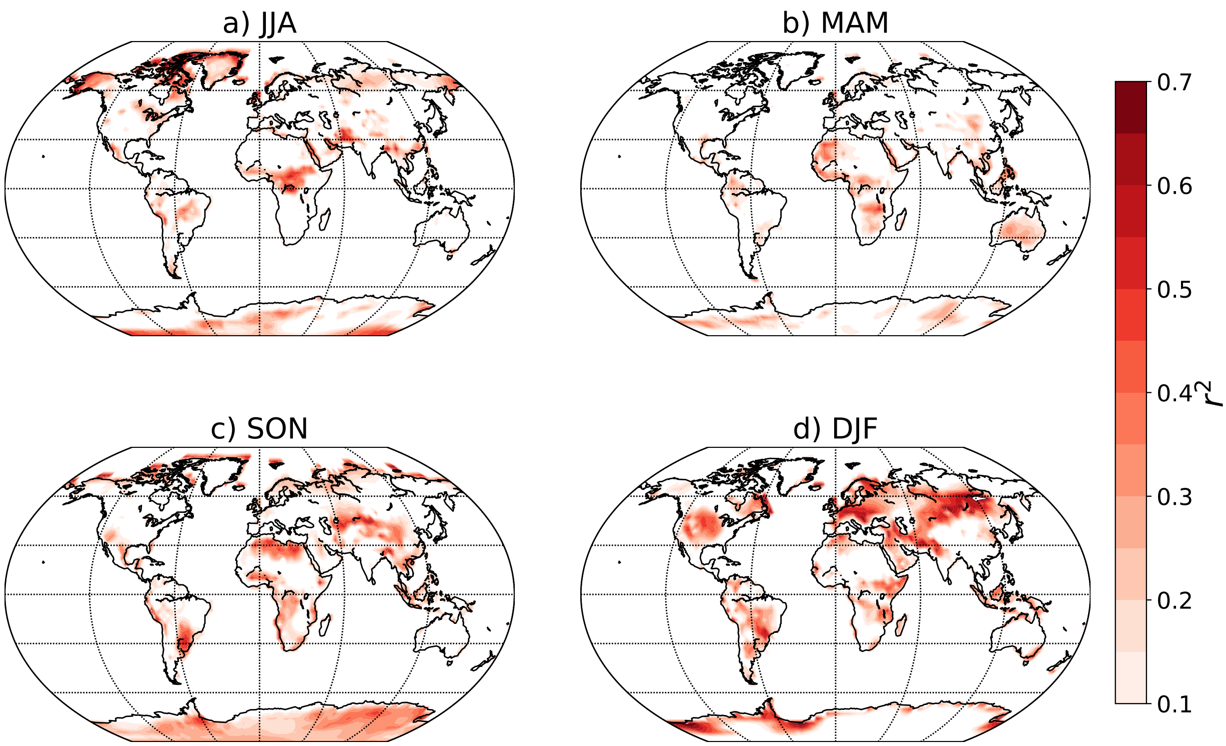

602 FIG. 6. a) r^2 values for correlations across the CMIP6 models between baseline JJA q_v (i.e., averaged over years 1-10) and JJA $\Delta\theta_E$. Only values over land, with $r^2 > 0.1$, are plotted. b) but for MAM. c) Same as panel a) but for SON. d) Same as panel a) but for DJF values.

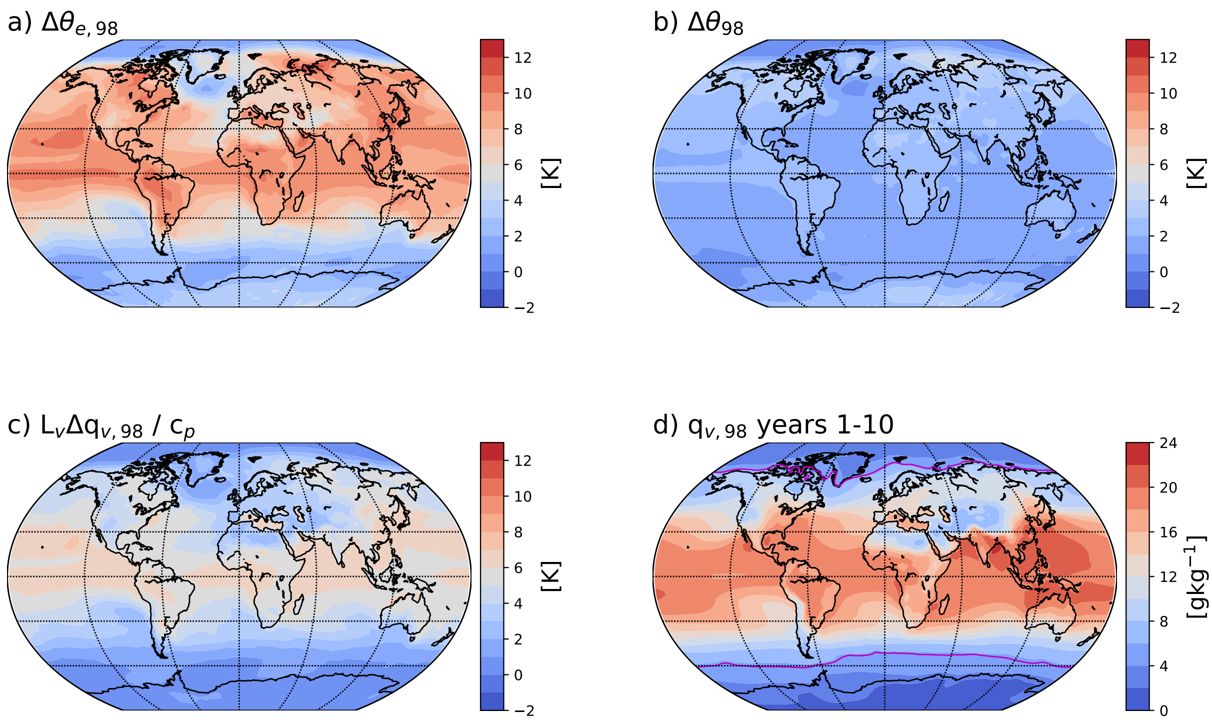

FIG. 7. a) Composite changes in the 98th percentile of daily θ_E between years 71-80 and years 1-10 in transient warming simulations with 14 CMIP6 models. b) Composite changes in θ, conditioned on the 98th percentile of θ_E. c) Composite changes in q_v, multiplied by $\frac{L_v}{c_p}$ and conditioned on the 98th percentile of θ_E. d) Baseline q_v, conditioned on the 98th percentile of θ_E, averaged over years 1-10 of the simulations. The magenta contours show the 5.6gkg^{-1} isopleth.

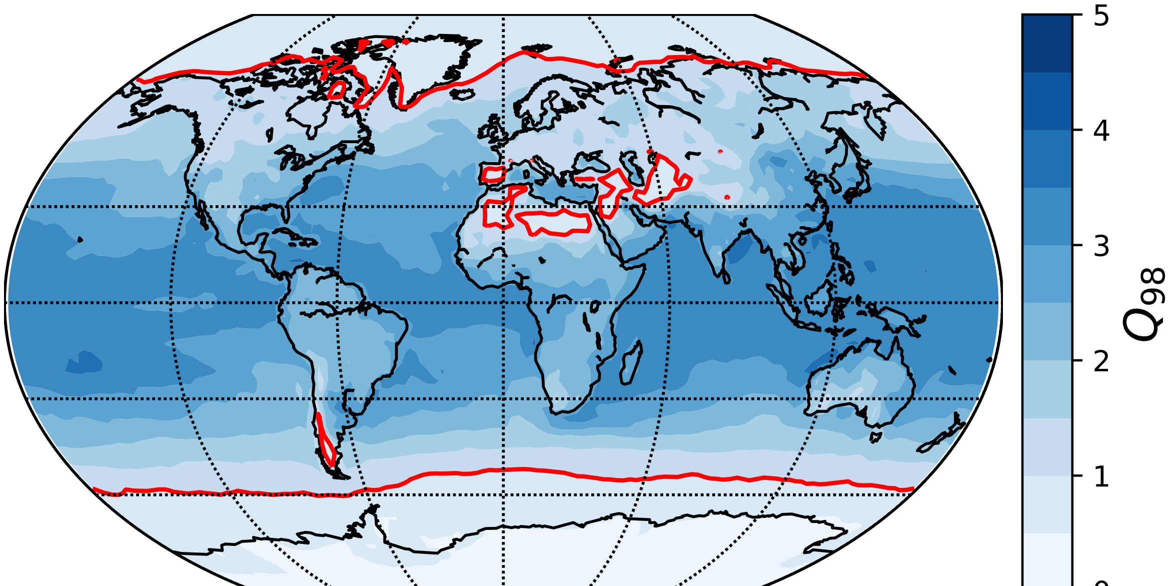

FIG. 8. The ratio $Q_{98} = L_v \Delta q_{v,98}/c_p \Delta\theta_{98}$ for the multi-model composite response of the 14 CMIP6 models.

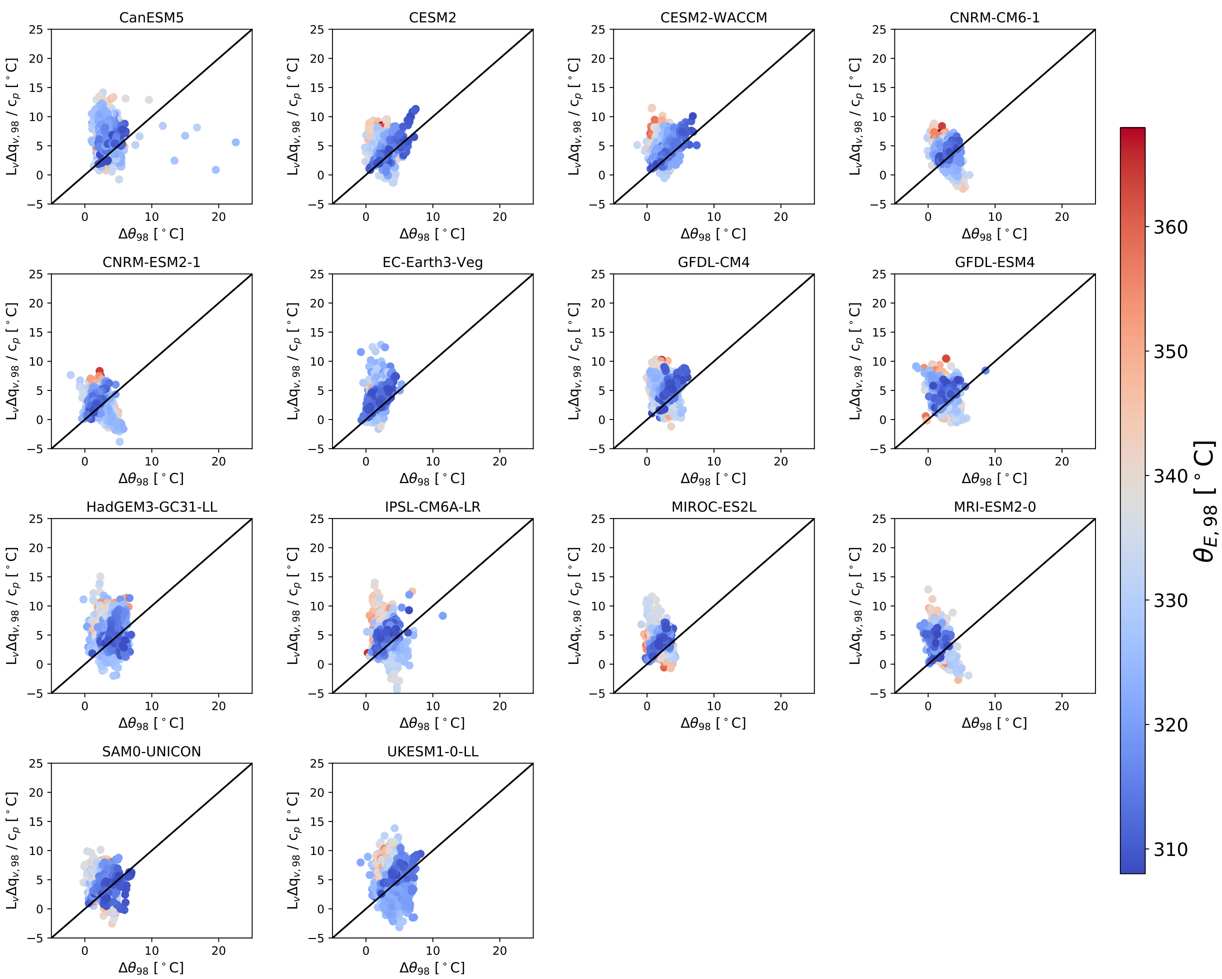

610 FIG. 9. Scatter plots for the 14 CMIP6 models of changes in specific humidity ($L_v \Delta q_{v,98}/c_p$) versus changes
611 in temperature ($\Delta\theta_{98}$) associated with 98th percentile θ_E events that are $\geq$308K. The markers are colored by
612 their associated $\theta_{E,98}$ value in the baseline climate.

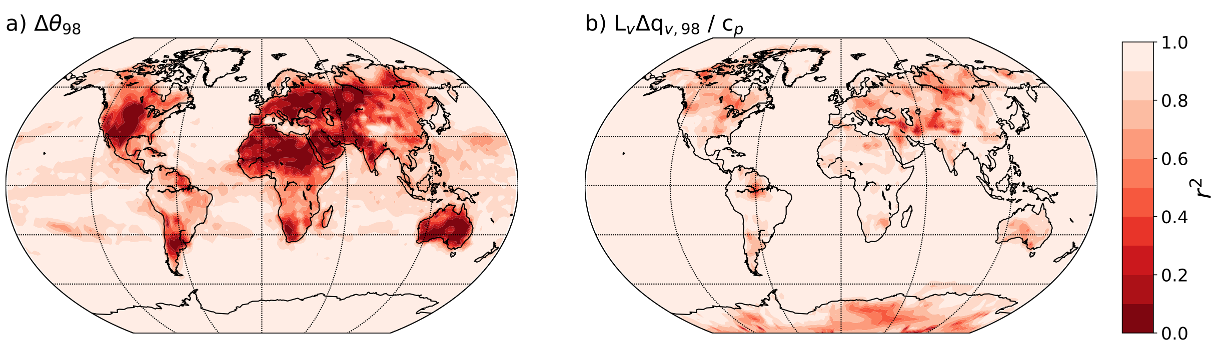

613 FIG. 10. a) r^2 values for correlations across the CMIP6 models between $\Delta\theta_{E,98}$ and $\Delta\theta_{98}$. b) r^2 values for correlations across the CMIP6 models between $\Delta\theta_{E,98}$ and $\Delta q_{v,98}$.

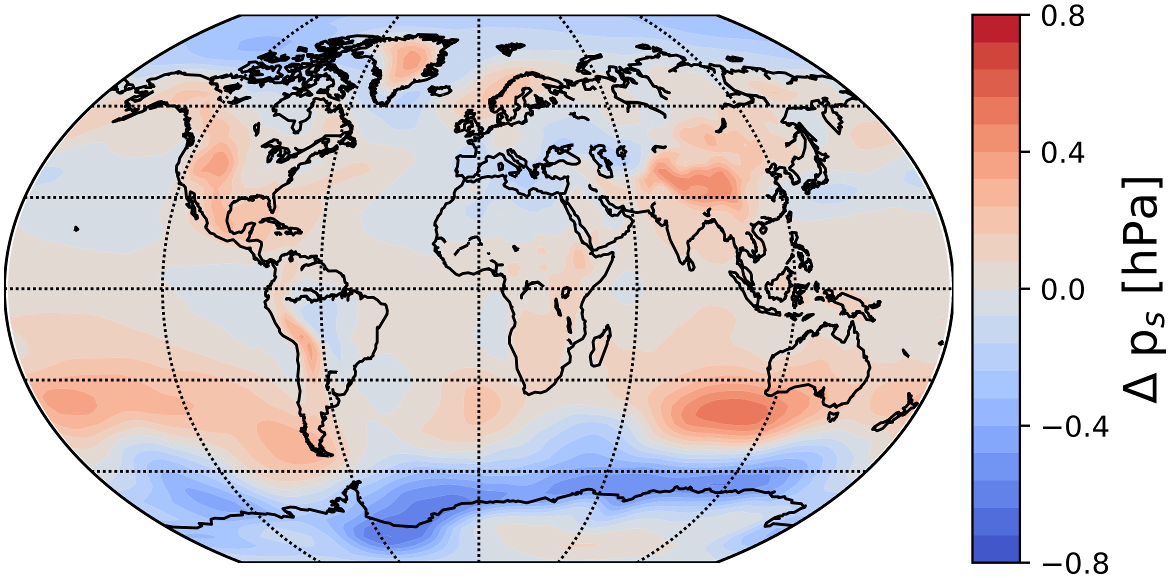

615 FIG. 11. Composite changes in JJA surface pressure between years 71-80 and years 1-10 in transient warming
616 simulations with 14 CMIP6 models.